ELSEVIER

Cement & Concrete Composites 24 (2002) 65–72

Cement & Concrete Composites

www.elsevier.com/locate/cemconcomp

# Macrocell corrosion of steel in concrete – implications for corrosion monitoring

B. Elsener [1]

*Institute of Materials Chemistry and Corrosion, Swiss Federal Institute of Technology, ETH Hönggerberg, CH-8093 Zurich, Switzerland*

**Abstract**

Macrocell corrosion with a local anode and a large cathode frequently occurs in chloride induced corrosion of rebars in concrete and is responsible for very high local corrosion attacks and reduction in cross-section found e.g., in bridge decks or substructures. In model-macrocells in electrolytes and in mortar the influence of the conductivity and cover depth on potential and macrocell current distribution have been studied both in open circuit conditions and under external anodic polarisation. The results have shown that low electrolyte conductivity and low cover facilitate the location of the anode of the macrocell by potential measurements due to a concentration of the spreadout of the macrocell action. Under anodic polarisation the imposed current is concentrated on the local anode. The consequences for corrosion monitoring by half-cell potential mapping and by polarisation resistance measurements on locally corroding rebars are discussed. 

*Keywords:* Corrosion; Concrete; Corrosion monitoring

## 1. Introduction

Reinforcing steel in good quality concrete does not corrode even if sufficient moisture and oxygen are available. This is due to the spontaneous formation of a thin protective oxide film (passive film) on the steel surface in the highly alkaline pore solution of the concrete. When sufficient chloride ions (from de-icing salts or from seawater) have penetrated to the reinforcement or when the pH of the pore solution drops to low values due to carbonation, the protective film is destroyed and the reinforcing steel is depassivated. Corrosion in the form of rust formation and/or loss in cross-section of the rebars occur in the presence of oxygen and water (humidity) [1–3]. The corrosion of steel in concrete essentially is an electrochemical process, where at the anode iron is oxidised to iron ions that pass into solution and at the cathode oxygen is reduced to hydroxyl ions. Anode and cathode form a short-circuited corrosion cell, with the flow of electrons in the steel and of ions in the pore solution of the concrete [1–3].

According to the different spatial location of anode and cathode, corrosion of steel in concrete can occur in different forms:

- as *microcells*, where anodic and cathodic reactions are immediately adjacent, leading to uniform iron dissolution over the whole surface. Uniform corrosion is generally caused by carbonation of the concrete or by very high chloride content at the rebars.
- as *macrocells*, where a net distinction between corroding areas of the rebar (anode) and non-corroding, passive surfaces (cathode) is found. Macrocells occur mainly in the case of chloride induced corrosion (pitting), generally the anode is small respect to the total (passive) rebar surface.

On reinforced structures and in the experimental study of macrocells, coplanar or face to face situations of anode and cathode can be distinguished [4–6]. A typical coplanar situation is a localised corrosion attack in an otherwise passive rebar (Fig. 1), a typical face to face situation is the corroding upper layer of the reinforcement in a bridge deck with the lower mat being passive. Macrocell corrosion is of great concern because the local dissolution rate (reduction in cross-section of the rebar) may greatly be accelerated due to the large cathode/anode area ratio [4–6]. Indeed, values of local corrosion rates up to 1 mm/year have been reported for bridge decks, sustaining walls or other chloride

[1] Present address: Department of Inorganic and Analytical Chemistry, University of Cagliari, Monserrato, I-09042, Cagliari, Italy. Tel.: +39-070-675-4464; fax: +39-070-675-4456.

0958-9465/02/$ - see front matter 
PII: S0958-9465(01)00027-0

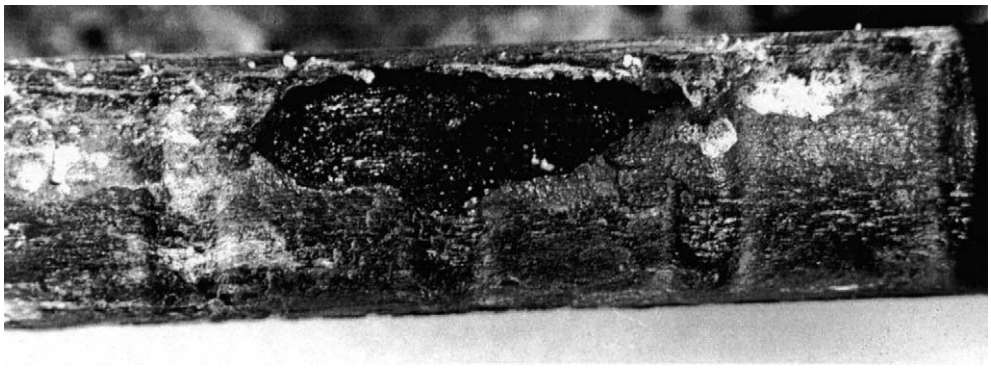

Fig. 1. Localised corrosion attack on a 20 mm rebar, loss in cross-section ca. 30%.

contaminated RC structures [7–9]. This rapid corrosion attack may lead – if not detected early to structural safety problems.

Corrosion monitoring by half-cell potential mapping allows to locate precisely and in an early stage the anode of macrocell action by identifying local minima in the measured potential field at the concrete surface [7,10,11, and literature cited therein]. It is generally recognised that fixed boundry values (e.g., −0.35 V CSE) to identify corroding zones cannot be applied [11]. The conductivity of the concrete and the cover depth influence both the potential readings at the concrete surface and the possibility to detect small corrosion attacks. The instantaneous corrosion rate of steel in concrete can be determined by linear polarisation resistance measurements [12,13, and references cited therein] and a good correlation between the electrochemical weight loss calculated by integration of polarisation resistance ($R_p$) data and the gravimetric weight loss was found in laboratory experiments. The same technique can be applied on reinforced concrete structures; there, the area of the counter electrode is much smaller than that of the working electrode (rebars) and the electrical signal vanishes with increasing distance from the counter electrode. Numerical methods based on transmission line models [14] or the use of a guard ring (second concentric counter electrode to confine the applied current beneath the central CE) [15] are used to overcome this difficulty and the instantaneous corrosion rate $i_{corr}$($\mu$A cm$^{-2}$) can be determined correctly [9,16,17]. The significance of such $i_{corr}$ values in the case of macrocell or localised corrosion with high local loss in cross-section of the rebars (Fig. 1) is still under discussion [17]. Experimental data from on-site measurements have shown that in the frequent case of chloride induced, very localised corrosion attacks (Fig. 1) occurring in chloride contaminated concrete, the average corrosion rates determined from $R_p$ measurements underestimate the real, local penetration rates by a factor of 5 to 10 [9].

In this work, the influence of cover depth and conductivity on the macrocell current and potential distribution is studied using model-macrocells in water and in mortar. The results are discussed with respect to consequences for corrosion monitoring by half-cell potential mapping and polarisation resistance measurements.

## 2. Experimental

### 2.1. Model bar for macrocell corrosion

The experiments simulating localised corrosion in an active/passive macrocell were performed on a macrocell bar (total length 0.4 m) with a central anode of mild steel (3 cm$^2$) and 12 lateral cathodes (16 cm$^2$) of stainless steel 1.4301 on both sides (Fig. 2). With the bar diameter of 2 cm results a characteristic geometry with surface to length ratio of 6.3 cm$^2$/cm. The total area ratio of

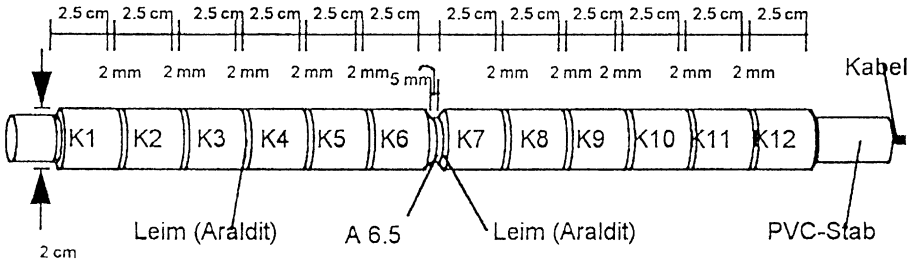


Fig. 2. Schematic representation of the macrocell bar with anode (mild steel) and segmented cathodes (SS 1.4301).

cathode to anode is 60. The anode and the 12 cathodes were mounted on an electrically isolated plastic bar with a slot for the connecting wires. Anode and cathodes could be short-circuited externally. The total macrocell current and the currents to the individual cathode segment currents were measured with a zero resistance ammeter, and the switching was performed on a programmable multimeter (Keithley). A special switchboard guaranteed a complete short circuit during the measurements. Data were recorded on a personal computer. The corrosion potentials of the anode and cathodes were measured with a saturated calomel electrode (SCE). In an additional series of experiments the response of the macrocell bar to anodic polarisation with galvanostatic pulse was measured with the same arrangement.

### 2.2. Experiments in water

One of the bars was mounted in a small tank ($0.4 \times 0.2 \times 0.2$ m$^3$) in order to perform experiments in water where the cover could be varied easily by filling the tank to different heights, usually 2 or 3 cm above the bar. The macrocell bar was fixed at a height (with respect to the bottom) of 7 cm. Aqueous solutions with different conductivities were used to simulate different concrete resistivities (Table 1). In water, in addition to the total macrocell current and the current distribution on the individual cathode segments, potential profiles were measured at different heights above the bar by scanning a reference electrode along the bar.

### 2.3. Experiments in mortar

Two macrocell bars were embedded in PC mortar using 500 kg of cement/m$^3$ and a water cement ratio of 0.5. 3% chloride as NaCl was added to the mixing water. The mortar blocks were cured for one week in a humidity cabinet and then exposed to the laboratory atmosphere. The dimensions of the mortar blocks were $0.4 \times 0.1 \times 0.1$ m$^3$ and the cover over the bar was 20 (MPK1) and 30 mm (MPK2), respectively. On the mortar blocks potential profiles at the surface, total macrocell current and the current distribution on the individual cathode segments were measured.

## 3. Results

### 3.1. Macrocell under open circuit conditions

#### 3.1.1. Resistance in the macrocell

The resistance between the central anode and the individual lateral cathodes was measured (AC 1 kHz). After multiplication by the conductivity of the electrolyte, a normalised resistance $R^*\sigma$ is obtained and the influence of geometry (distance from anode and cover depth) can be observed (Fig. 3). It can be stated from Fig. 3 that the normalized resistance $R^*\sigma$ measured in the water tank is identical for the different specific conductivities of the electrolyte, the three curves measured in water coincide and have the same characteristic, symmetrical shape showing an increase of the resistance with distance from the anode. The two mortar blocks with a slightly different geometry (smaller cross-sections, thus smaller volume) show higher normalised resistance values (Fig. 3). The mortar block MPK1 with the lower cover of 20 mm shows the highest values.

#### 3.1.2. Potential profiles

The resulting potential profiles measured along the macrocell bar at a cover depth of 20 mm are shown in

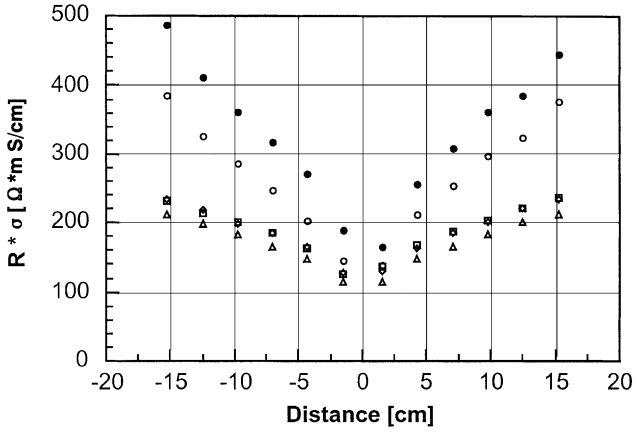


Fig. 3. Normalized resistance $R^*_\Omega\sigma$ between anode (position 0) and cathode segments in distilled water (◇), tap water (Δ), dilute sulfate solution (□), and in the two mortar blocks MPK1 (cover 30 mm) ○, and MPK2 (cover 20 mm) (●).

Table 1
Values of conductivity and specific resistance of the different electrolytes used (Mixed water is a mixture of distilled water and tap water)

| Medium | Symbol | Conductivity (μS cm$^{-1}$) | Resistivity (Ω m) | Resistivity (Ω cm) |
|---|---|---|---|---|
| Distilled water | DW | 7 | 1300 | 130,000 |
| Mixed water | MW | 70 | 130 | 13,000 |
| Tap water | TW | 360 | 27 | 2,700 |
| Mortar blocks | MPK | 430 | 22 | 2,200 |

Fig. 4 for the different electrolytes. The highest resistivity of the electrolyte (distilled water, 1300 Ω m) shows the most pronounced potential difference between anode and cathodes, with decreasing resistivity the potentials become more and more similar. Cathode segments close to the anode shows more negative potentials, this effect is more pronounced in low resistive electrolytes (Fig. 4). In the extreme case of the mortar block (22 Ω m), all the cathodes, irrespective of the distance from the anode, show the same potential as the local anode.

In distilled water (1300 Ω m) potential profiles were measured at different heights above the macrocell bar (Fig. 5). Decreasing the distance from 20 (cover depth) to 0.5 mm the potential profiles become more pronounced: the potential measured above the anode decreases and the potentials measured above the individual cathode segments become more positive.

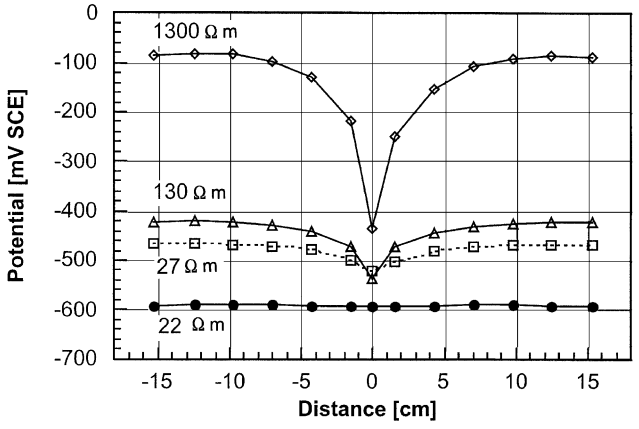


Fig. 4. Potential profiles measured along the macrocell bar (cover 20 mm) for the same solutions as in Fig. 3. Solution resistivity is indicated in the figure.

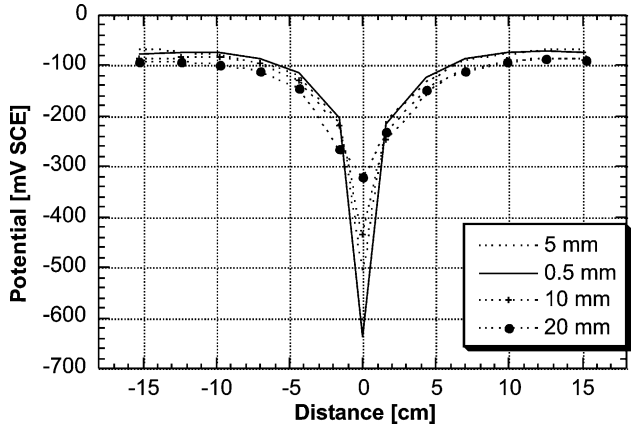


Fig. 5. Potential profiles measured along the macrocell bar (cover 20 mm) in distilled water (1300 mm) at different heights above the bar (0.5, 5, 10 and 20 mm). Anode at position 0.

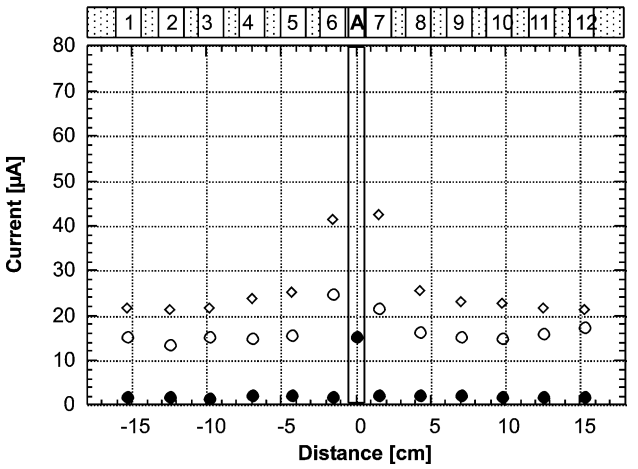


Fig. 6. Distribution of the cathodic currents in the macrocell for different conductivities of the solution, cover 20 mm (mixed water, ○ tap water, ● mortar block MPK1). The anode current for mixed water was 310 μA, tap water 200 μA and mortar block 16 μA.

### 3.1.3. Total current and current distribution

The current distribution in the macrocells is shown in Fig. 6. The total current flowing in the macrocell (equal to the anode dissolution current) increases with increasing conductivity, current densities on the anode between 60 and 450 $\mu A/cm^2$ are measured in aqueous solutions. Despite the low resistivity of the mortar blocks a macrocell current of only 16 μA (respect to the anode 5 $\mu A/cm^2$) were measured. The current distribution on the cathode segments is symmetrical (Fig. 6), the cathodic currents are highest close to the anode and decrease with increasing distance from the anode. For electrolytes with medium to high conductivity, the macrocell bar used in this work is too short for a significant decrease of the cathodic current to be observed.

## 3.2. Macrocell under anodic polarisation

### 3.2.1. Resistance

The resistance between the CE and the macrocell, $R_{ME/CE}$, in a parallel plane arrangement was measured for the different electrolytes and cover depths used (Table 2). The resistance is proportional to the resistivity of the electrolyte and increases with increasing cover depth. Calculating the normalised resistance identical values are found for the experiments in water with different conductivities (Table 2). For the mortar blocks the resistance $R_{ME/CE}$ measured is clearly higher compared to the values that would correspond to the mortar resistivity (Table 2) due to the different volume of the mortar blocks and to the coupling of the CE to the concrete surface by means of a wet sponge.

Table 2
Resistance between counter electrode and macrocell bar (coplanar arrangement) and total resistance $R_{tot}$ between anode and cathodes for different electrolytes and cover depths

| Medium | Cover $d$ (mm) | $\sigma$ (mS/cm) | $R_{ME/CE}$ (Ω) | $R^*\sigma$ | $R_{tot}$ (Ω) | $R^*_{tot}\sigma$ |
|---|---|---|---|---|---|---|
| Distilled water | 20 | 0.02 | 567 | 11.3 | 4700 | 94 |
| | 30 | 0.02 | 860 | 17.0 | – | – |
| | 50 | 0.02 | 1146 | 22.5 | – | – |
| Tap water | 20 | 0.37 | 30.4 | 11.25 | 250 | 92.5 |
| | 30 | 0.37 | 41.1 | 15.2 | – | – |
| | 50 | 0.37 | 56.5 | 21.7 | – | – |
| MPK1 | 20 | 0.432 | 563 | – | 235 | 101.5 |
| MPK2 | 30 | 0.408 | 752 | – | 225 | 97.2 |

### 3.2.2. Current distribution at the macrocell under anodic polarisation

The partial currents in the anode and the different cathode segments of the macrocell bar after imposing an anodic current from the counter electrode at the surface are shown in Fig. 7. Most of the imposed anodic current (50 μA) flows into the (small) anode, only a small fraction flows to the cathodes. In mortar (Fig. 7) all the currents are anodic due to the low cathodic currents in the macrocell prior to application of the anodic current (Fig. 6). For a given conductivity of the solution the distribution of the imposed current to anode and cathodes depends on the cover depth (distance of the counter electrode from the macrocell bar). For covers of 50, 30 and 20 mm between 70% and 44% of the imposed current flows to the anode, it is only for low and very low covers, 10, 1 mm, that appreciable anodic current enters the cathodes (Table 3).

Looking at the time dependence of the partial currents, it can be observed that in the first 10 s the current measured at the anode increases, the current at the cathodes instead slightly decreases with time (Fig. 8).

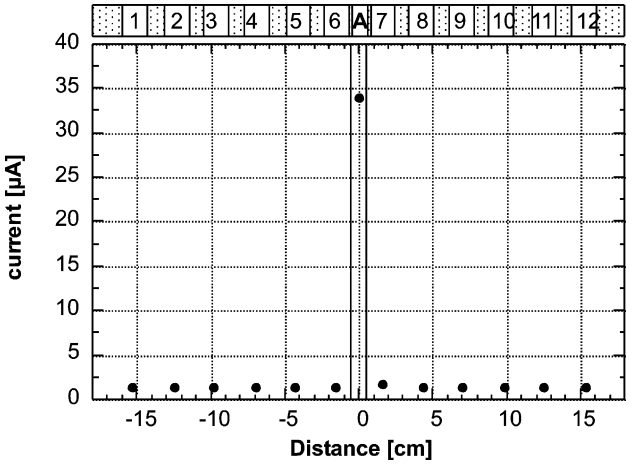


Fig. 7. Steady state current distribution on the anode and cathode segments of the macrocell bar in mortar (cover 20 mm) with galvanostatic anodic polarisation $I = 50$ μA from a counter electrode on the surface (plan parallel arrangement).

## 4. Discussion

Macrocell corrosion between actively corroding areas of rebars and large passive areas (either beside the active spot or behind in a second layer of reinforcement) is of great concern because it results in very high local anodic current densities with corrosion rates up to 0.5–1 mm/year [4,6,24]. The resulting local loss in cross-section has dangerous implications for the structural safety if the corroded rebars are located in a zone of high tensile or shear stresses. Furthermore, these dangerous attacks very often do not manifest themselves at the concrete surface by cracking or spalling because soluble iron chloride complexes are formed [22]. Thus it is of great importance how these locally corroding spots can be detected early and what the implications for the different

Table 3
Distribution of the imposed anodic current $I_{app}$ between the anode and the cathodes of the macrocell bar in distilled water (7 μS cm$^{-1}$) for different cover depths (distance between counter electrode and macrocell bar in plan parallal arrangement)

| Cover (mm) | $I_{app}$ (μA) | $I$ Anode (μA) | $I$ cathodes (μA) | % Anode |
|---|---|---|---|---|
| 50 | 50 | 35 | 15 | 70 |
| 30 | 80 | 55 | 25 | 68 |
| 20 | 80 | 35 | 45 | 44 |
| 10 | 200 | 60 | 140 | 30 |
| 1 | 300 | 60 | 240 | 20 |

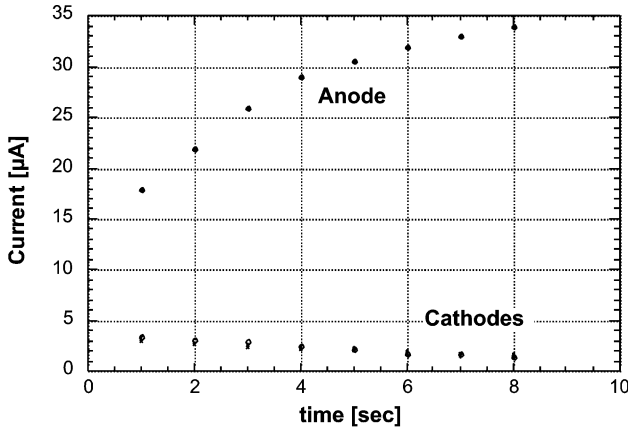


Fig. 8. Change of partial currents of the anode and the cathode segments of the macrocell bar in mortar (cover 20 mm) with time of polarisation. Galvanostatic current pulse $I = 50$ μA.

corrosion monitoring techniques as half-cell potential mapping or polarisation resistance measurements are. The mechanism of these corrosion attacks in the form of macrocells has already been discussed [4–6].

### 4.1. Half-cell potential mapping

The difference between the potential of the anode and the cathodes – up to 0.5 V have been measured in this work in aqueous electrolytes, in chloride containing wet mortar about 0.3 V were found – allows the location of the corroding spots from the concrete surface. Similar results are reported in literature [5,18]. Several points have a significant influence on the half-cell potential measurements.

- *Cover depth*: with increasing cover depth the potential values measured over active and passive areas become more similar (Figs. 4 and 5) thus the location of small corroding spots becomes more difficult as already stated.
- *Concrete resistivity*: in high resistive concrete the highest potential difference between anode and cathodic areas are measured (Fig. 4). This helps – in principle – to detect corroding spots. Contrary only a small cathode area around the anode is polarised to negative potentials (Fig. 4). Thus in high resistive concrete small corroding spots can be found only with a very small grid size of potential mapping. In humid, chloride contaminated concrete with low resistivity a much larger cathodic area is polarised to negative potentials (Fig. 4) and the location of the small anode is possible with a large grid size.

From the experiments it can further be observed that the macrocell bars used in this work in electrolytes with medium to high conductivities are too short to reach unaffected cathodic areas. Only in distilled water is the resistance high enough to focus the macrocell action in the region of ±15 cm, which represents an anode to cathode ratio of 1:30 on each side. Despite the high conductivity of the mortar blocks (0.43 mS/cm) and their similar geometry (primary resistance Fig. 3) the macrocell currents measured are 10–20 times lower than in aqueous solutions (Fig. 6). This can be explained by the much lower cathodic current densities found in mortar respect to solutions as reported elsewhere [23], the reason might be the restricted oxygen access to the cathodes in the very humid, chloride containing mortars. Thus in mortar or concrete the primary resistance distribution is controlling the macrocell current only at high resistivity of the concrete and if oxygen is readily available, in the case of chloride induced corrosion the cathodic reaction is controlling the overall reaction in the macrocell [24].

### 4.2. Polarisation resistance measurements

The evaluation of the corrosion rate from polarisation resistance measurements in real structures is of great importance for the assessment of corrosion risk to existing structures or for residual life time predictions. The DC polarisation resistance technique with IR compensation and calculation of the instantaneous corrosion current, $i_{corr}$, has been applied extensively since 1970 by Andrade, Feliù and co-workers [12,13] to study the corrosion of steel in concrete. In the case of a localised corrosion attack (small anode in a large cathode bar) with local loss in cross-section of the rebars (Fig. 1) or macrocell corrosion in general two main difficulties arise.

- *Position of the counter electrode*: The position of the locally corroding area (anode) of the rebars can be located with half-cell potential mapping. The imposed steady state (anodic) current from the counter electrode put on the concrete surface mainly flows into the corroding area (see Fig. 7). This is due to the fact that the imposed current tends to follow the path of lowest total resistance, thus the current will flow to the anode because (a) the distance is shortest and (b) the polarisation resistance of the anode $R_p$ is very low (note that the specific polarisation resistance $R_p^*$ of the anode is several 100 times lower than $R_p^*$ of the passive rebars [12,17]). If the counter electrode on the concrete surface is moved laterally away from the corroding area and again a polarisation resistance measurement is performed, the imposed current will still flow mainly to the anode as long as the total resistance is lower than that for the current to enter into rebars in the passive state (high $R_p$). In practice this means that low $R_p$ values are measured also when the CE is placed above completely passive areas if a corroding anode is closeby. The size of the corroding

area as determined from $R_p$ measurements might be overestimated. By using a second concentric counter electrode (guard ring) the current flow can be confined to the area under the central CE [15,16] and errors due to this macrocell effect can be reduced if the size of the concentric counter electrode is much larger then the cover depth and the CE is placed on homogeneous passive rebars (away from the anode in the macrocell) [20].

- *Localised corrosion rate*: The measured electrochemical response of the system (polarisation resistance) provides little or no indication of the localised nature of corrosion. On first approximation, it could be assumed that the result of $R_p$ measurement is due to a uniform corrosion of the steel surface examined (equal to the CE area put on the concrete surface). In the case of a localised corrosion situation the excitation current coming from the counter electrode on the concrete surface enters predominantly the active areas (hot spots, Fig. 7) has been shown also by simulation calculation with an electrical network [17,20], the corrosion and the current distribution on the macrocell is not uniform. Thus the assumption of uniform corrosion leads to a significant underestimation of the real corrosion rate at the anode irrespective the use of CE with or without guard ring. Numerical simulation for several geometric arrangements and cathode/anode ratios have shown that the error can reach nearly a factor of 10 [17,20].

An additional problem to be considered is the variation of current distribution between anode and cathodes in the macrocell with the frequency of the imposed current [17,19]. The non-uniform DC distribution on the macrocell (Fig. 7) has been found to change to a uniform current distribution at high frequencies (e.g., 1 kHz) [17,19] because at high frequencies the impedance of steel in concrete is determined mainly by the interfacial capacitance, nearly equal on actively corroding and on passive areas. The same results can be observed in this work the time domain (Fig. 8): at short times ($\ll$1 s) less than 30% of the total applied current are flowing to the anode, in the steady state more then 70%. This uniform current distribution at high frequencies (or equivalent very short time) leads to a significant error in the determination of the ohmic resistance of the system: at high frequencies (e.g., 1 kHz) or very short times (e.g., in pulse measurements) the measured ohmic resistance $R_p$ is determined by the size of the counter electrode as shown by field measurements [17,21] and numerical simulations [19,20] – the actual resistance to the flow of DC current (see Fig. 7) is much higher and is determined by the size of the anode [17,19]. Because in high resistive media as concrete the measured polarisation resistance $R_p$ has to be corrected for the contribution of the ohmic resistance (subtracting $R_p$) this underestimation of $R_p$ leads to an overestimated, IR-free polarisation resistance $R_p$ and thus, applying the usual reciprocal relationship, again to an underestimation of the real corrosion rate of the anode. This is an inherent problem of $R_p$ measurements on non-uniformly corroding metals, it cannot be avoided by using a guard ring.

## 5. Conclusions

In real structures with localised chloride induced corrosion macrocells are formed that greatly accelerate the local dissolution rate of the anode. From this work performed on active/passive model-macrocells with measurements of the resistance, potential and current distribution in the macrocell the following conclusions regarding corrosion monitoring can be obtained

1. The location of the corroding anode by determination of the minimum in the half-cell potential map is facilitated in principle by higher concrete resistivity and lower cover depth. For practical application of half-cell potential mapping with a large grid size of the measuring points, small anodic areas are located better in low resistive media (e.g., chloride contaminated concrete) due to the strong cathodic polarisation of passive rebars close to the anode.
2. Most of the DC current applied by an external counter electrode on the concrete surface placed over the active/passive macrocell flows to the local anode despite the large cathode area (anode/cathode area ratio 1:60). Thus polarisation resistance measurements on locally corroding rebars will result in an erroneous corrosion rate of the anode, the error can arise to a factor of 10.

## References

[1] Tuuti K. Corrosion of Steel in Concrete, CBI Forskning/Research. Cement och Betonginstitutet: Stockholm; April 1982.
[2] Schiessl P. Corrosion of Steel in Concrete, RILEM Technical Committe 60-CSC. New York: Chapman & Hall; 1988.
[3] Elsener B. Corrosion of steel in concrete. In: Schütze M, editor. Corrosion and Environmental Degradation, vol. II, Wiley-VCH: Weinheim; 2000. p. 389–436.
[4] Andrade C, Maribona IR, Feliu S, Gonzalez A, Feliu Jr. S. Corrosion Science 1992;33:237.
[5] Raupach M. Chloride induced macrocell corrosion of steel in concrete – theoretical background and practical consequences. Construction and Building Materials 1996;10:329.
[6] Elsener B, Hug A, Bürchler D, Böhni H. Evaluation of localized corrosion rate on steel in concrete by galvanostatic pulse technique. In: Page CL, Bamforth PS, Figg JW, editors. Corrosion of Reinforcement in Concrete Construction. SCI; Cambridge: 1996. p. 264–272.

[7] Elsener B, Böhni H. Potential mapping and corrosion of steel in concrete. In: Berke NS, Chaker V, Whiting D, editors. Corrosion Rates of Steel in Concrete ASTM STP1065. Philadelphia: American Society for Testing and Materials; 1990. p. 143.
[8] Hunkeler F. Assessment of corrosion on RC structures with potential mapping. Schweiz Ingenieur und Architekt 1991;109:272 [in German].
[9] Elsener B. Corrosion rate on reinforced concrete structures determined by electochemical methods. Materials Science Forum 1995;192–194:857.
[10] Elsener B, Böhni H. Location of corroding rebars in concrete structues. Schweiz Ingenieur und Architekt 1987;105:528 [in German].
[11] Elsener B. Draft on half-cell potential mapping, RILEM TC-154, Materials and Structures. Submitted.
[12] Feliu S, Gonzalez JA, Andrade C, Feliu V. Determining polarization resistance in reinforced concrete slabs. Corrosion Science 1989;29:105–13.
[13] Andrade C, Castelo V, Alonso C, Gonzales JA. The determination of the corrosoin rate of steel embedded in concrete by the polarization resistanc and AC impedance methods. In: Chaker V, editor. Corrosion Effect of Stray Currents and the Techniques for Evaluating Corrosion of Rebars in Concrete. Philadelphia: ASTM STP 906; 1986. p. 43.
[14] Feliu S, Gonzales JA, Andrade C, Feliu V. On-site determination of the polarization resistance in a reinforced concrete beam. Corrosion NACE 1988;44:761.
[15] Feliu S, Gonzales JA, Andrade C, Rz-Maribona I. In: Page CL, Treadaway KW, Bamforth PB, editors. Corrosion of Reinforcement in Concrete. London: Elsevier Applied Science; 1990. p. 293.
[16] Andrade C, Alonso C, Feliù S, Gonzalez JA. Applications of corrosion rate values. In: Blankvoll A, editor. Proceedings of International Conference on Repair of Concrete Structures. Nordland: Norwegian Publlic Roads Administration; 1997. p. 365–74.
[17] Elsener B. Corrosion rate of steel in concrete – from laboratory to reinforced concrete structures. In: Mietz J, Elsener B, Polder R, editors. Corrosion of Reinforcement in Concrete, Monitoring, Prevention and Rehabilitation. London: The Institute of Materials IOM Communications; 1998. p. 92–103.
[18] Alonso MC, Andrade C, Farina J, Lopez F, Merino P, Novoa XR. Galvanic corrosion of steel in concrete. Materials Science Forum 1995;192–194:899–906.
[19] Sagüés AA, Kranc SC. Computer modeling of effect of corrosion macrocells on measurement of corrosion rates of reinforcing steel in concrete. In: Berke NS, Escalante E, Nmai C, Whiting D, editors. Techniques to Assess the Corrosion Activity of Steel Reinforced concrete Structures. ASTM STP1276. American Society for Testing Materials; 1996. p. 58–73.
[20] Kranc SC, Sagüés AA. Computation of corrosion macrocell current distributin and electrochemical impedance of reinforcing steel in concrete. In: Munn RS, editor. Computer Modeling in Corrosion, ASTM STP 1154. American Society for Testing and Materials; 1992. pp. 95–112.
[21] Elsener B, Flückiger D, Wojtas H, Böhni H. Methods to Assess Corrosion of Steel in Concrete Report 521, Verein Schweiz. Strassenfachleute, Zürich 1996 [in German].
[22] Guilbaud JP, Chahbazian G, Derrien F, Raharinaivo A. Electrochemical behaviour of steel under cathodic protection in medium simulating concrete. In: Swamy RN, editor. Corrosion and Corrosion Protection of Steel in Concrete, vol. 2. Sheffield Academic Press; p. 1382–1391.
[23] Sykes JM. Materials Science Forum 1995;192–194:833–42.
[24] Raupach M, Gulikers J. Investigations on cathodic control of chloride induced reinforcement corrosion. In: Proceedings of the EUROCORR 1999 (on CD). Aachen; 1999.